Measuring changes in tissue oxygen metabolism due to radiotherapy in patients with brain metastases

Jordi de Leeuw[1], Eva van Grinsven[2], Jeroen Siero[3,4], Mariëlle Philippens[5], Junghun Cho[6], Alex Bhogal[3]

[1]Imaging division, UMC Utrecht, Netherlands, [2]Department of Neurology & Neurosurgery, UMC Utrecht, Netherlands, [3]Department of Radiology, UMC Utrecht, Netherlands, [4]Spinoza Center for Neuroimaging, Amsterdam, Netherlands, [5]Department of Radiation Oncology, UMC Utrecht, The Netherlands [6]SUNY Buffalo, Buffalo, NY, United States.

Abstract - ***Radiotherapy might have an influence on the homeostatic regulation of tissue in the brain. The ratio of deoxygenated versus oxygenated blood in the venous blood vessels, namely the oxygen extraction fraction (OEF), might be a promising method to give insights of radiotherapy-related changes in brain metabolism. The cerebral metabolic rate of oxygen ($CMRO_2$) can be inferred from OEF and the cerebral blood flow (CBF). These three parameters provide an indication of tissue health. Eleven patients with brain metastases were scanned prior to and after radiotherapy (RT). Scans included structural scans as well as susceptibility weighted imaging (SWI) and arterial spin labelling (ASL) acquisitions based on which, OEF, CBF and $CMRO_2$ maps were calculated. Regions of interest (ROIs) were created of healthy tissue as well as malignant tissue and in accordance with the amount of delivered dose. The Wilcoxon rank test and Friedman test were executed on these ROIs and their respective values of OEF and $CMRO_2$. Results suggest an overall increase of $CMRO_2$ after radiotherapy in brain tissue (excluding tumors). Additionally, a significantly lower OEF was found in tumor tissue compared to healthy tissue indicating an altered metabolism in malignant tissue. In conclusion, The data provides a clear implication of the use of OEF and $CMRO_2$ and their change after radiotherapy as well as their importance as biomarkers for general tissue health and indication of malignant areas.***

Index terms - Cerebral metabolic rate of oxygen ($CMRO_2$), oxygen extraction fraction (OEF), magnetic resonance imaging (MRI), quantitative blood oxygenation level-dependent imaging (qBOLD), quantitative susceptibility mapping (QSM), susceptibility, QSM+qBOLD (QQ),

I. INTRODUCTION

A. Homeostatic Regulation of The Vascular System

The human brain plays a crucial role in the regulation and coordination of various bodily functions and requires a substantial amount of energy to carry out its complex operations. It has been estimated that the brain is responsible for approximately 20% of the basal metabolic rate of the body, making it the most energetically demanding organ[1], [2].To realize this vast amount of energy, the brain primarily relies on aerobic metabolism[3]. The primary sources of energy for this process are oxygen and glucose, which are supplied to the brain via the bloodstream[4], [5].

However, various diseases such as stenotic occlusive diseases and those that damage or change the cerebrovascular system can lead to a reduction in the blood supply to the brain, thereby affecting its energy supply. In such circumstances, the brain uses autoregulatory mechanisms to maintain a healthy baseline energy supply[1], [6]. These mechanisms include an increase in cerebral blood flow (CBF) through vasodilation, and an increase in the oxygen extraction fraction (OEF)[6].

If the normal homeostatic regulation of the vascular system in the brain is not sufficient to

meet the energy demands of the brain, the brain may resort to a change in metabolism in order to fulfill its oxygen and nutrition demands[7]. An example of a change in metabolism is when engaging in high-intensity physical exercise, where the body shifts its metabolism from aerobic metabolism to anaerobic metabolism[8]. However, if the autoregulatory mechanisms and metabolic reprogramming are inadequate, tissue damage may occur leading to a range of consequences including cell death and eventually cognitive impairments[9].

Furthermore, malignant tissue such as a brain tumor, may alter the homeostatic regulation of the vascular system in the brain since tumor tissue has a different metabolism than healthy brain tissue[10]. Whereas regular cells rely on aerobic glycolysis, tumor cells tend to use an altered form of aerobic glycolysis for quick energy supply, known as the Warburg effect[5]. Next to that, brain tumors are characterized by rapid and disorganized angiogenesis[11]. This disorganized angiogenesis leads to increased oxygen diffusion distances and areas of hypoxia (Figure 1)[12]. As a result, an increased OEF is necessary to compensate for these areas of decreased oxygen delivery and ensure that the tumor has adequate oxygen and nutrient supply[12].

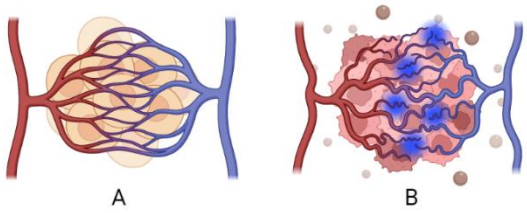

Figure 1: Microvasculature in healthy tissue (A) versus the microvasculature in tumor tissue (B). In tumor tissue, disorganized angiogenesis leads to areas of hypoxia, indicated in blue. The areas of hypoxia demand a higher OEF from neighboring veins to ensure sufficient oxygen and nutrient supply[12]*. Created with BioRender.com*

One of the main treatments for brain tumors is cranial radiotherapy (RT) which ought to destroy the disorganized vasculature of brain tumors with high-energy radiation[11]. However, the radiation might also (un)intentionally irradiate healthy brain tissue, as a result of which the delicate microvasculature might also be damaged[13]. Studies have found that a dose of above 10 Gy delivered to tissue has a severe influence on the vascular system, leading to vascular damage and therefore decreased blood perfusion in the brain[13]. Other studies have found a reduction in cerebral blood flow (CBF) at radiation doses less than 10 Gy[14]. Next to vascular damage, the immune response of apoptosis might be triggered at doses of 5 to 10 Gy and necrosis might occur in tissue that has received doses of above 10 Gy[15].

Taking the effects of malignant tissue and radiotherapy on OEF and CBF into consideration, it is essential to understand the regulation of energy metabolism in the brain and the role of autoregulatory mechanisms in maintaining its health under various physiological and pathological conditions.

B. Importance of OEF and $CMRO_2$ as Biomarker

Since the brain's ability to store oxygen is limited, it primarily relies on extracting oxygen from incoming arterial blood in real-time to meet its oxygen demands[16]. This makes OEF a very direct measure of the brain's oxygen uptake and therefore could be a potential biomarker. Additionally, when combined with CBF, OEF can be expressed as the cerebral metabolic rate of oxygen ($CMRO_2$) which indicates the homeostatic regulation of the brain and is therefore another valuable biomarker[2], [17]. Research suggests $CMRO_2$ to remain unchanged in healthy tissue at most times as OEF and CBF are in balance[18]. However, when the microvasculature in the tissue is damaged, in case of (un)intentional irradiation of brain tissue, the brain may not be able to increase CBF to particular brain areas through vasodilation[19]. The close neurovascular coupling might then be disrupted, rending the vessels unable to dilate, while still being able to restrict blood flow[19]. As a result, OEF has to increase for $CMRO_2$ to remain unchanged or increase slightly[12]. In addition, due to the rapid growth of malignant tissue, elevated $CMRO_2$ values are expected in tumor areas, leading to a significant increase in OEF as a result of increased perfusion to hypoxic regions

and the disorganized vasculature within the tumor[12]. Furthermore, since tumor microenvironment is comprised of both malignant and nonmalignant cells, and the tumor cores are often poorly perfused, it is expected that OEF and CMRO2 values in the tumor location may be very heterogeneous[11], [20].

On the contrary, $CMRO_2$ values in malignant tissue may also appear unaltered due to the Warburg effect. Warburg et al. discovered this effect, in which there is a switch from normal oxidative phosphorylation that uses oxygen to create energy, to aerobic glycolysis that converts glucose to lactate to produce ATP[5], [10], [12], [21]. When the Warburg effect has become dominant in tumor tissue, the consumption of oxygen might appear normal[12].

Accordingly, the relationship between OEF and $CMRO_2$ and their respective change due to vascular damage or rearrangement is an important indicator for tissue health and damage after radiotherapy.

C. OEF and $CMRO_2$ Measurements

Multiple modalities can be used to measure the oxygen extraction fraction. Previously, a PET scan with ^{15}O-labeled radiotracers was considered to be the golden standard for measuring the oxygen extraction fraction[16]. However, due to the patient exposure to ionizing radiation, other diagnostic techniques such as MRI-based methods have gained increasing preference.

This research uses a quantitative susceptibility mapping (QSM) approach with quantitative blood oxygen-level dependent imaging (qBOLD). This combination, referred to as QQ, has been suggested to produce similar results in OEF compared to the previously used ^{15}O-PET in healthy patients[22]. The basic principle for QSM relies on changes in the amount of de-oxyhemoglobin (dHb) permeating the brains tissues. The unbound Fe^{+} atom in dHb leads to localized susceptibility-related field disturbances that can be probed via QSM techniques[22]. Using the QQ method with temporal clustering, tissue composition and total variation (QQ-CCTV), OEF values can be calculated from these quantitative susceptibility maps[22], [23]. By combining the OEF with CBF data, $CMRO_2$ maps can be generated.

D. Research Question

Given that high-energy radiation can potentially cause vascular damage in the brain, investigating the impact of radiotherapy on the health of brain tissue is of scientific interest. In particular, the relationship between $CMRO_2$ and OEF is a useful indicator of brain tissue health. Given that the novel QQ-CCTV method has proven to be a feasible and reliable method for non-invasively measuring OEF, this study will employ the QQ-CCTV method and aim to characterize the changes in OEF and $CMRO_2$ in brain tissue due to radiotherapy[23]. Hence, we will examine how the OEF and $CMRO_2$ values in both healthy tissue and malignant areas are related before and after radiotherapy, as well as the changes that occur in each area. In addition, using dose maps, the influence of different dose levels on OEF and $CMRO_2$ values in healthy tissue will be investigated in order provide a more comprehensive understanding of radiation-induced damage to healthy tissue.

I. METHODS

A. Patients and Inclusion Criteria

A dataset was used from the ongoing study Assessing and Predicting Radiation Influence on Cognitive Outcome using the cerebrovascular stress Test (APRICOT). This study includes a growing amount of patients with brain metastases, who voluntarily apply for inclusion in this study. At the time of this analysis, the dataset contains 26 patients of which 17 patients have successfully completed a pre- and post-radiotherapy MRI session. The pre-radiotherapy scanning session was planned on the same day and before the radiotherapy session while the post-radiotherapy session was planned between three and four-and-a-half months after the radiotherapy. From these 17 patients, six patients were excluded for this study due to incomplete data or severe (motion) artefacts in the susceptibility weighted images. The eleven patients in the remaining dataset

ranged in age from 52 to 81 years and included 6 males (Mean age = 69 years) and 5 females (Mean age = 62 years).

B. Data Acquisition

Patients were scanned on a Philips 3T MRI system using a 32 channel Nova receive coil. Along with structural images such as T1 weighted- and a T2FLAIR scan, the scan protocol also included (1) resting susceptibility weighted imaging (SWI) using the following imaging parameters: flip angle = 17 degrees, number of slices = 63 , voxel size = 0.342 x 0.342 x 2 mm, TR = 50 ms, scan resolution = 384 x 383, number of echos = 5, TE1 = 8.5ms, TE5 = 44.5ms, echo spacing = 8ms , FOV = 230 x 126 x 189 mm, Bandwidth in readout direction = 177.4Hz/px. Total scan duration = 393 seconds and (2) a baseline multi-delay pseudo-continuous 2D arterial spin labeling acquisition was performed (PCASL): 4 post-labeling delays = 660, 1325, 1989, 2654 ms, readout = Look-Locker EPI, label duration = 1650 ms, TR = 5s, TE = 12 ms, flip angle = 25°, acquired resolution: 3.5 x 3.5 x 7 mm, acquisition matrix: 80 x 80 x 17, 23 dynamics, SENSE factor = 2, 2 background suppression pulses.

C. Data Processing

Raw phase and magnitude data provided QSM maps and were calculated with the Sepia toolbox using projection onto Dipole Field (PDF) as background field removal technique and the Morphology enabled dipole inversion (MEDI) toolbox[24]–[26]. See Figure 2. The resulting QSM and the multi-echo 3D-GRE (magnitude/phase) data were then used to generate OEF maps using the QQ-CCTV method of Cho et al.[23], [27]. Next to that, CBF maps (mL/100 g/min) were generated from ASL data to create the $CMRO_2$ maps (µmol/100g/min) in combination with the OEF data according to the following equation:

$$CMRO_2 = OEF * CBF * [H]_\alpha \qquad (1)$$

In which $[H]_\alpha$ is the oxygenated heme molar concentration in the arteriole expressed in µmol/ml. In this study, an oxygenated heme molar concentration of 7.377 µmol/ml is used in accordance with research by Zhang et al.[27].

Prior to further processing, several segmentations were generated. Edema masks for pre- and post-RT were semi-automatically generated based on the T1 and T2FLAIR images using the lesion growth algorithm as implemented in the Lesion Segmentation Tool

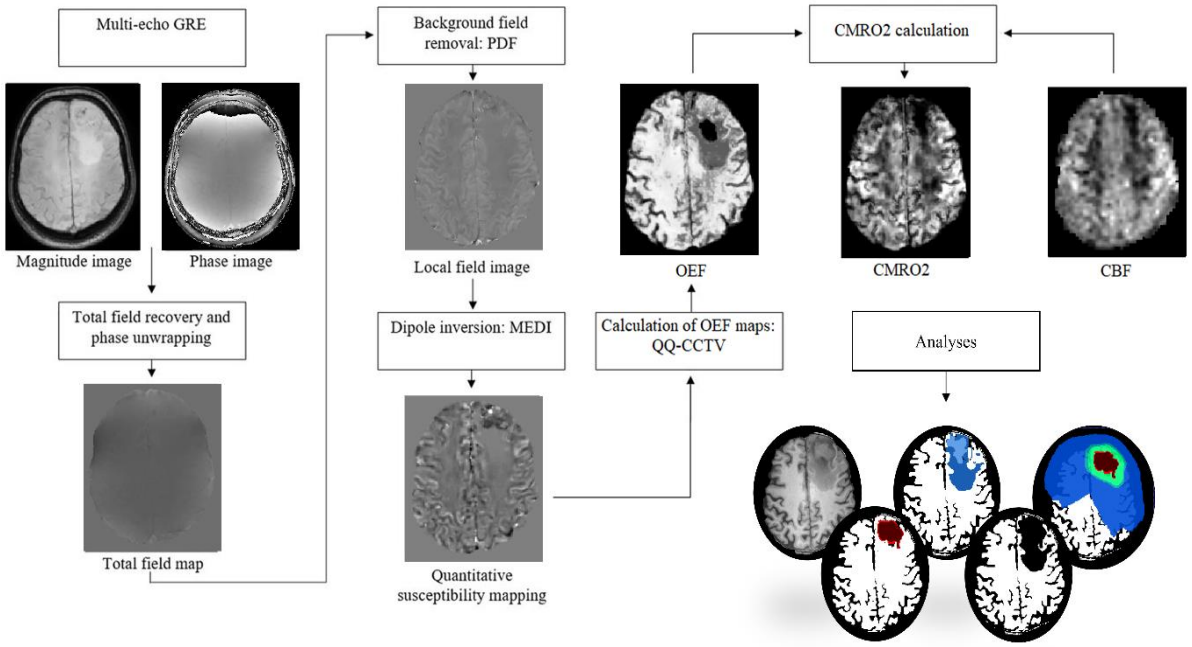

Figure 2: pipeline for creating QSM, OEF and CMRO2 images from raw phase and magnitude data using the SEPIA toolbox with the PDF and MEDI toolbox [24]–[26]

(LST, https://www.statistical-modelling.de/lst.html) for SPM[28]. An initial threshold of 0.14 was applied. The resulting edema mask was manually modified to exclude any false positives or false negatives from the LST edema mask. Additionally, the T1 weighted scan was brain extracted using the FSL BET tool and used as a reference for creating the whole brain mask and the CSF mask[29], [30]. The whole brain masks and CSF masks were automatically generated by the FSL FAST algorithm based on this brain extracted T1 weighted image[31], [32].

Furthermore, dose maps and tumor delineations were extracted from each patient. These maps and delineations were retrieved from the radiotherapy department at which the tumor masks are delineated based on pre radiotherapy CT scans, acquired one to five days before receiving radiotherapy. From the tumor delineations, a malignant tissue mask was generated which included both the planned tumor volume (PTV) of metastases, resection cavities and PTV of tumors irradiated prior to the APRICOT to ensure all non-healthy tissue was included. For accurate comparison of tumor volume pre- and post-radiotherapy, only the gross tumor volume (GTV) was used.

Prior to further processing, all of the created images and masks were registered and interpolated to align to the brain extracted T1 weighted scan of the pre-RT scanning session using the FSL FLIRT algorithm[33], [34].

To correctly identify healthy tissue, the whole brain mask was used after excluding cerebrospinal fluid (CSF), edema of the pre- and post-RT scan and malignant tissue. Additionally, a whole brain mask was used excluding only CSF and malignant tissue, while preserving edematous areas hereinafter referred to as 'semi-healthy tissue mask'. The application of this mask allowed for the identification of the impact of radiotherapy on both healthy tissue and the development or resolution of edema.

To investigate the effects of radiotherapy on brain tissue, the dose maps were discretized to create three areas receiving a different dose. A low dose area was created of tissue that received less than 10 Gy with a minimum of 0.5 Gy. This lower threshold of 0.5 Gy was chosen to ignore all zero dose areas and was set in

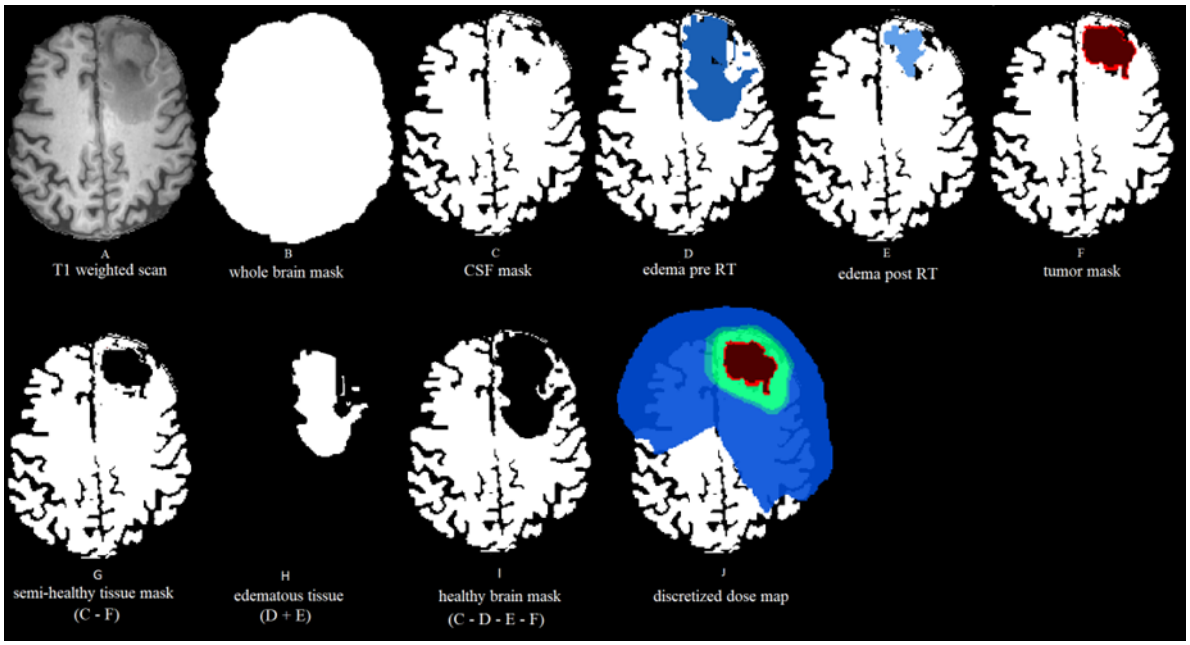

Figure 3: used segmentations and subsequent developed masks. A) T1, B) whole brain mask, C) CSF, D) pre-RT edema, E) post-RT edema, F) PTV, G) mask excluding malignant tissue but preserving edematous areas (semi-healthy tissue mask), H) edematous tissue mask, I) healthy brain mask, J) discretized dose map and PTV(red) with in blue (between 0.5Gy and 10Gy), light green (between 10Gy and 15Gy) and green (>15Gy) based on criteria described in Park et al.[13].

accordance with literature, which states that a dose of 0.5 Gy is too low to trigger apoptosis[35]. Next to the low dose area, a medium dose area was created between 10 Gy and 15 Gy and a high dose area was created of tissue that received more than 15 Gy in accordance with the observations of Park *et al.* and Haikerwal *et al.* [13], [15].

For a detailed overview of the used segmentations and subsequent developed masks, see Figure 3.

Furthermore, subtraction images were generated to examine alterations in OEF and $CMRO_2$ following radiotherapy (RT). This was accomplished by subtracting the pre-RT scanning session data from that of the post-RT scanning session. The subtraction process was restricted to pixels that contained values in both the pre- and post-RT images. Moreover, due to the QQ-CCTV method occasionally producing OEF and $CMRO_2$ values in cerebrospinal fluid (CSF), which is generally inappropriate, the resulting image was masked to exclude CSF. Additionally, outliers were excluded since there might be some motion artefacts and misalignment with respect to the B0 field of the patient between the sessions which creates problems for dipole inversion of the QSM data. The criterion used for this was three times the standard deviation. At last, due to the aforementioned variabilities in measurements, values in close proximity to zero were considered as zero values using a threshold criterion of 0.2 times the standard deviation. Examples of OEF, $CMRO_2$ and the related subtraction images can be found in Figure 4. For more examples, see Appendix A, Figure 8.

D. ROI and Statistical Analysis

The dataset of OEF and $CMRO_2$ values was created with in-house scripts using MATLAB version 2022b (The MathWorks Inc., Natick, Massachusetts). Statistical analyses were then performed using SPSS version 28 (IBM Corp., Armonk, New York). Comparisons of OEF and $CMRO_2$ between pre-RT and post-RT were performed in specific regions of interest (ROIs). The analysis was performed in conjunction with a discretized dose mask and ROIs separated into healthy tissue, 'semi-healthy tissue', gross tumor volume (GTV) and edematous areas.

For each patient, the mean, standard deviations and the voxel count per ROI was calculated for both OEF and $CMRO_2$. All ROI calculations that are based on less than 0.1% of the total amount of voxels in the whole brain mask were excluded. Due to the small sample size ($n = 11$), the Wilcoxon signed rank test was used to assess significant differences between means of OEF or $CMRO_2$ with a significance level of $p < 0.05$. A Bonferroni correction was applied when doing multiple comparisons to account for Type II errors resulting in an alpha value of $\alpha = 0.025$. Since the Wilcoxon signed

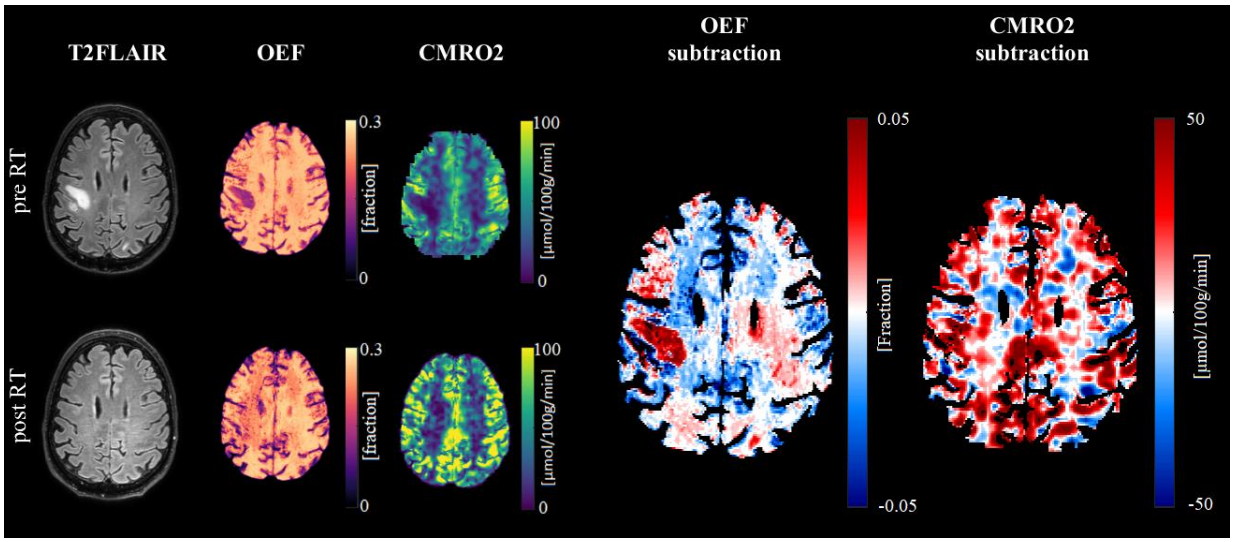

Figure 4: examples of calculated OEF and CMRO2 maps pre- and post-radiotherapy, including the associated subtraction maps with outliers removed and values close to zero set to zero to account for variabilities in measurements.

rank test is a nonparametric test, no tests for normality were conducted on the variables.

In order to evaluate the impact of received dose on OEF and $CMRO_2$ in (ROIs), difference scores were extracted from the subtraction images and subjected to statistical analysis in the ROI of healthy tissue while also considering the discretized administered dose. For this analysis the nonparametric Friedman test was used. Post-hoc tests were conducted using the Wilcoxon signed-rank test with Bonferroni correction for multiple comparisons. Since the low-dose areas are relatively large compared to the healthy tissue that received a high dose, the ROI calculations were executed and analyzed with both the mean and the median of the data to examine and prevent the possible major influence of outliers.

After thorough exclusion of all severe motion artefacts, three cases remained in the dataset with very little motion artefacts. These were included in statistical analysis. However, the same analyses were also conducted excluding these cases to investigate if the exclusion of these patients would lead to significant different results.

II. Results

A. Malignant Tissue Compared to Healthy Tissue Prior and Post Radiotherapy

A Wilcoxon signed-rank test was conducted to examine the differences in the OEF and $CMRO_2$ between healthy tissue and tumor tissue *prior* to cranial radiotherapy. The results showed that the OEF was significantly higher in healthy tissue (M = 0.19) compared to tumor tissue (M = 0.14), (Z = -2.366, $p < 0.05$). See Figure 5. However, the $CMRO_2$ did not significantly differ between healthy tissue and tumor tissue (Z = -1.214, $p = 0.225$).

Subsequently, a Wilcoxon signed-rank test was conducted to examine the differences in OEF and $CMRO_2$ between healthy tissue and tumor tissue after radiotherapy. The results showed that, similar to the pre-radiotherapy results, there was a statistically significant higher OEF in healthy tissue (M = 0.19) compared to tumor tissue (M = 0.13; Z = -2.028, $p < 0.05$). Furthermore, the Wilcoxon signed-rank test for $CMRO_2$ after radiotherapy yielded a non-significant difference between healthy tissue and tumor tissue (Z = -1.782, $p = 0.075$). See Appendix B, Figure 9.

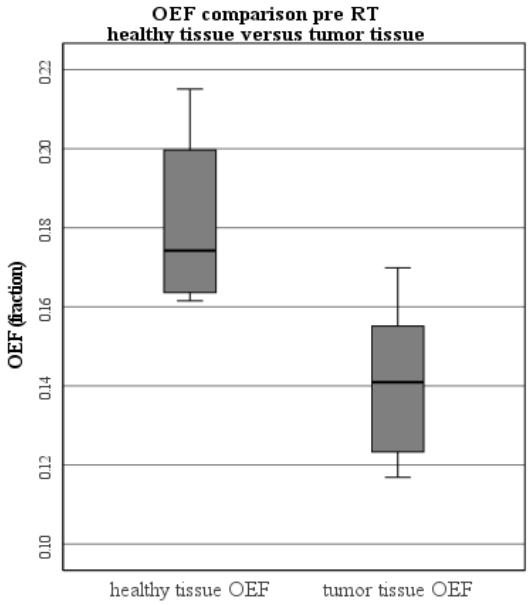

Figure 5: OEF comparison pre radiotherapy in healthy tissue versus tumor tissue. Results indicated a significant higher difference in OEF between healthy tissue (M =0.19) and tumor tissue (M = 0.14; Z = -2.366, p < 0.05).

B. Malignant Tissue Prior Radiotherapy versus Malignant Tissue After Radiotherapy

To investigate changes in OEF and $CMRO_2$ at the location of malignant tissue after radiotherapy, Wilcoxon signed-rank tests were conducted. The results showed no statistically significant difference in OEF between pre-radiotherapy (M = 0.14) and post-radiotherapy (M = 0.13) in malignant tissue (Z = -0.579, $p = 0.562$). Similarly, there was a non-significant difference in $CMRO_2$ between pre-radiotherapy (M = 39.9) and post-radiotherapy (M = 38.9) in malignant tissue (Z = -0.405, $p = 0.686$). See Appendix B, Figure 10.

C. Semi-healthy Tissue Prior to Radiotherapy versus Semi-healthy Tissue After Radiotherapy

To investigate possible differences in semi-healthy tissue post-RT compared to pre-RT

semi-healthy tissue, a Wilcoxon signed-rank test was conducted. In semi-healthy tissue, a nonsignificant difference in OEF between pre- and post-radiotherapy with a z-value of Z = -0.889 and p = 0.374. A further Wilcoxon signed-rank test on the differences in healthy tissue post-RT compared to pre-RT as well as in edematous areas with the applied Bonferroni correction yielded no significant results; (Z = -0.978, p = 0.328) and (Z = -1.156, p = 0.248) respectively.

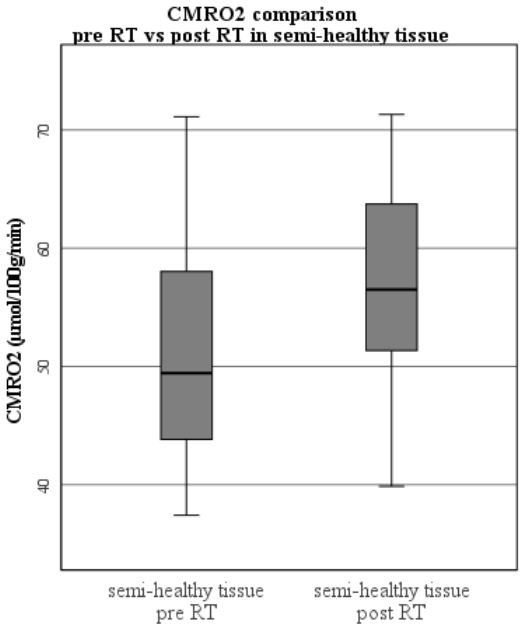

Figure 6: CMRO2 comparison in semi-healthy tissue before and after radiotherapy. Results indicated a significant increase in CMRO2 in semi-healthy tissue after radiotherapy (M = 58.3) compared to before radiotherapy (M = 52.3; Z = -2.045, p < 0.05).

However, in the case of CMRO2, a statistically significant higher CMRO2 was found in the semi-healthy tissue post-radiotherapy (M = 58.3) compared to pre-radiotherapy (M = 52.3) with a z-value of (Z = -2.045, p < 0.05). See Figure 6. A further investigation was executed to compare the effects of healthy tissue and edematous tissue. The Bonferroni correction was applied resulting in an alpha value of 0.025. These tests yielded a non-significant difference of CMRO2 for both healthy tissue of pre-radiotherapy compared to post-radiotherapy (Z = -2.045, p = 0.026) and edematous areas (Z = -1.274, p = 0.203). See Appendix B, Figure 11.

D. Change of OEF and $CMRO_2$ in Healthy Tissue Based on Delivered Dose

The Friedman test revealed that the changes in OEF and $CMRO_2$ mean values of healthy tissue before and after radiotherapy did not significantly differ based on the radiation dose received by the tissue. For the OEF, the Friedman test resulted in a chi-square value of $X^2(2) = 1.273$ with a p-value of 0.529, while for $CMRO_2$, the test resulted in a chi-square value of $X^2(2) = 0.6$ with a p-value of 0.741. The Friedman test on changes in OEF and $CMRO_2$ based on the median of the data did not provide different results. See Figure 7.

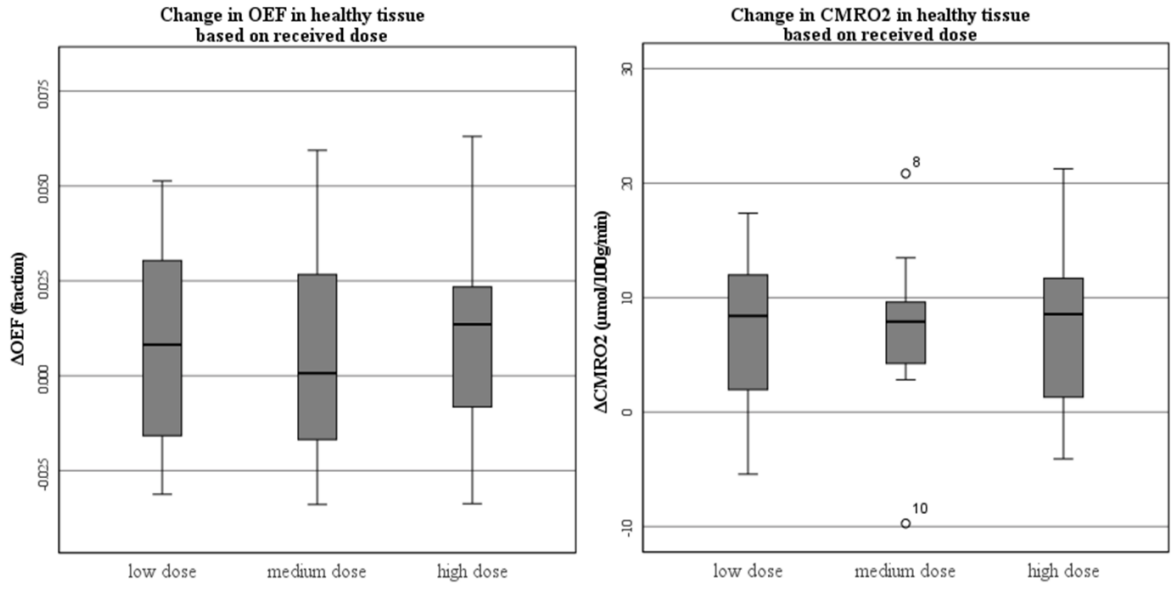

Figure 7: Change in OEF and CMRO2 in healthy tissue according to the dose received. Healthy tissue was subdivided in three areas, receiving a low-, medium- or high dose. Results indicated no significant differences across the three dose levels for both OEF and CMRO2, ($X^2(2) = 1.273$, $p = 0.529$) and ($X^2(2) = 0.6$, $p = 0.741$), respectively.

E. Additional Analyses Excluding Patients with Minor Motion Artefacts

When excluding three patients of which minor motion artefacts are known in the QSM data, the result of the Wilcoxon signed-rank test of $CMRO_2$ in semi-healthy tissue post-RT compared to pre-RT, which previously indicated a significant higher difference in $CMRO_2$ after radiotherapy, changed to a nonsignificant higher difference ($Mean_{preRT}$ = 54.3, $Mean_{postRT}$ = 56.4, Z = -1.120, p = 0.263, n = 8). All other analyses did not differ in significance after excluding the three patients with minor motion artefacts.

III. DISCUSSION

This study aims to characterize the changes in OEF and $CMRO_2$ in brain tissue due to radiotherapy-induced vascular damage using the novel QQ-CCTV method[23]. Our main findings were a significantly higher $CMRO_2$ in semi-healthy brain tissue after radiotherapy, there were no significant differences in healthy tissue among the different dose levels we investigated and we found a significantly lower OEF in tumor tissue compared to healthy tissue.

The first observation is that after radiotherapy, the brain tissue excluding malignant areas (i.e. semi-healthy brain tissue) is more active in terms of $CMRO_2$ than prior to radiotherapy. Studies have found that exposure to radiation leads to an inflammatory response of the tissue[36], [37]. Therefore, it is possible that the increased metabolic activity of this semi-healthy brain tissue after radiotherapy is due to compensatory mechanisms, whereby the tissue is attempting to repair itself following radiation-induced damage. Since the OEF was not significantly increased, $CMRO_2$ would be increased by an increase in CBF. However, an increase in CBF is unexpected since we expect radiotherapy to damage blood vessels. As a result, the close neurovascular coupling might then be disrupted, rendering the vessels unable to increase blood flow[19].

We could not get a better insight into what kind of tissue was responsible for this increase in $CMRO_2$, being healthy tissue or edematous tissue. If the increase in $CMRO_2$ would be due to a significant increase in healthy tissue, the results would indicate inflammation of this tissue[36]. On the other hand, if the increase in $CMRO_2$ would be a result of a significant increase of $CMRO_2$ in edematous tissue, the results would indicate a resolution of edema [38], [39]. Nevertheless, these findings do suggest that radiotherapy does increase the overall $CMRO_2$ of brain tissue, excluding malignant brain areas.

Since the aforementioned analysis investigates the general treatment effect rather than the influence of dose on healthy tissue, a distinction was made to investigate the relationship of delivered dose on healthy tissue. We observed an insignificant variation in $CMRO_2$ among the various dose thresholds. This result is in line with our expectations and literature, which suggests that despite radiation-induced tissue damage, the brain's autoregulatory mechanisms try to maintain a constant level of $CMRO_2$[18].

However, we are aware of literature that reports most tissue vasculature can suffer irreversible damage if exposed to a dose exceeding 15 Gy[13]. Therefore, in order to maintain the same level of cerebral metabolism, we would expect an increasingly higher OEF across the different dose levels, based on equation (1). However, we did not find a significant difference in OEF across the three dose thresholds. With the aforementioned theory, we would have at least expected to find a statistical significant difference between OEF for low dose areas compared to high dose areas.

As OEF and $CMRO_2$ did not show a significant difference depending on different dose levels, it can be inferred that CBF also has not changed substantially with varying dosages. An explanation for this is found in previous research which shows that CBF might decrease even at doses lower than 10 Gy, implying that the changes in CBF at the different dose thresholds might be too minimal to be significant[14], [40]. Another possible explanation could be that most of the healthy tissue receives a low radiation dose, while a very small proportion of healthy tissue receives

a high dose. This could lead to a bigger influence of outliers in the smaller ROIs. Therefore, the ROI calculations were executed and analyzed with both the mean and the median values of the data, which for this analysis did not result in different outcomes. Future research might obtain more insightful results by distinguishing between two dose levels using other thresholds instead of three levels. Additionally, it is conceivable that, especially for low dose areas, tumor vasculature had recovered to pre-RT levels during the post-RT scan. Literature on mice carcinoma indicates that perfusion in tumor tissue experiences an initial decrease, but subsequently recovers to pre-radiation therapy levels after a certain period[13].

Furthermore and contrary to our expectations, the results show a lower OEF in tumor tissue compared to healthy tissue, both before and after radiotherapy. We had expected that prior to radiotherapy, the tumor would be in an active state to accomplish tumor growth. Due to the disorganized vasculature in tumor tissue, most of the increase in metabolic activity would then originate from an increase in oxygen extraction. Although after radiotherapy there was no notable difference in $CMRO_2$ between healthy- and tumor tissue, OEF remained significantly lower in tumor tissue compared to healthy tissue. We would expect this effect to have happened only after radiotherapy, since malignant tissue would be damaged and therefore less capable of responding to changes in oxygen demand or even begin to undergo necrosis. A possible explanation for these findings of lower OEF in tumor tissue could be that the Warburg effect, as explained earlier, is already dominant in the tumor metabolism. This effect states that the tumor would alter its glucose metabolism, making its energy production less reliant on oxygen[21]. This would then also explain why we did not find a significant difference in $CMRO_2$ values between healthy- and tumor tissue. Future research would take advantage of differentiating between the Warburg effect, or other forms of metabolism by introducing methods to measure metabolism. Since in the altered glucose metabolism, a vast amount of lactate is produced, the tumor cells would become more acidic[12][41]. This internal lactic acidosis can be picked up with proposed conventional MRI techniques and has an sensitivity of $\Delta pH = 0.03$[42]. Measuring the pH of tissue would then be a great additional value to distinguishing the type of used metabolism in cells. Additionally, measuring the pH of tissue would also provide evidence of inflammation in tissue, as an increase in pH is considered to be a sign of inflammatory processes[43].

Another useful technique which would indicate whether the Warburg effect is present would be to use MR spectroscopic imaging (MRSI). Where normal MRI relies on the abundant presence of hydrogen (^1H) to create anatomical images, spectroscopy images the chemical composition of a voxel. It mostly relies on the presence of hydrogen, but can also be used to image spectra with other molecules such as ^{31}P or ^{11}Na[44]. Recent literature specifically targeted the Warburg effect using MRSI based on deuterium (^2H)[45]. This novel method is already able to identify the Warburg effect in rat glioma models and would possibly be a great addition for distinguishing normal and abnormal metabolism in brain tissue[45].

Lastly, we looked at the tumor site and respective changes in OEF and $CMRO_2$ after radiotherapy. The findings suggest no significant difference in both OEF and $CMRO_2$ where we would have expected a decrease due to radiation-induced damage to the tissue. Nonetheless, because a tumor mask was not generated based on the post-radiotherapy scanning session, we cannot entirely attribute these findings to tumorous tissue. To illustrate, the tumor location could have changed in composition into a combination of necrotic tissue and newly generated healthy tissue. In that case, the change in OEF and $CMRO_2$ would depend on the state of activity of the normal brain tissue inside the tumor site. For a more accurate understanding of the changes in OEF and $CMRO_2$ in tumor tissue, future research should incorporate a second tumor mask which is generated at the moment of the scanning session after radiotherapy.

IV. LIMITATIONS

A major limitation of this research is the variations in the data that could be ascribed to variations in measurements and calculations. For example, in the creation of QSM images, the correct position of the head of the patient inside the main magnetic field (B_0) is very important for the dipole inversion method. Since we scan the patients at two timepoints, it is impossible to reproduce the exact same position of the head with respect to the B_0 field. Therefore, changes in QSM and subsequently subtle changes in OEF and $CMRO_2$ may be due to a variation in head position of the patient and therefore, the data has a low level of reproducibility.

Next to that, the calculation of OEF maps has proven to be very sensitive to values in the QSM map. Therefore, a subtle change in the QSM image could have a significant effect in the resulting OEF image. Motion artefacts during the creation of the SWI images could for example have a great influence on the resulting OEF maps. On top of that, in the QQ-CCTV analysis, the OEF image is scaled according to an automatically generated segmentation of the straight sinus mask based on the QSM image. If there were partial volume effects present in this segmentation, it would lead to distinct variations in the OEF image. An example of a possibly wrongly scaled image can be found in Appendix A, Figure 8, Patient 5.

Additional to the fluctuations in the data, the images were all registered to T1-space of the pre-radiotherapy scan. This could also have lead to minor changes in alignment between pre- and post-RT scans due to which, for example in the subtraction images, a major error margin has to be taken into account. Therefore, it was necessary to make adjustments to the subtraction maps for values close to zero. In the event that the variations in the data were less significant, a correspondingly smaller correction for values close to zero would suffice and the resulting data would be more accurate. Moreover, in the analysis of the subtraction maps, outliers were filtered with a criterion of more than three times the standard deviation. This resulted in mainly exclusion of malignant areas, since the OEF and $CMRO_2$ would be most affected in those places. However, as we did not account for these malignant areas when analyzing the impact of various dose levels on the tissue, we decided to maintain this criterion.

Finally, the analyses revealed a general increase in $CMRO_2$ in semi-healthy brain tissue. We could not attribute which part of the brain would be responsible for this increase, meaning either healthy tissue or edematous tissue. The statistical tests were carried out on the total edema mask, including voxels that contained either edema prior to radiotherapy or after radiotherapy. Since during the course of treatment, edema might have been resolved or grown, which is both possible due to the heterogeneity of patient responses included in the data, a distinction between new- and resolved edema would be of great interest. These values were included in the regional analyses. However, most of this data was excluded because it consisted of less than 0.1% of the total amount of voxels in that image.

V. CONCLUSION

In conclusion, the effects of radiotherapy on OEF and $CMRO_2$ in brain tissue differ from our initial expectations based on previous research. Presumably the presence of the Warburg effect in the analyzed patient data may explain the different outcomes for OEF and $CMRO_2$ in malignant tissue compared to healthy tissue. Results indicate that OEF is lower in malignant tissue than in healthy tissue, which is contrary to what literature would suggest. Next to that, tissue other than malignant areas showed a significant increase in $CMRO_2$, indicating either inflammation of the tissue or resolution of edema. Additionally, the applied dose thresholds did not result in significant differences in OEF or $CMRO_2$ whereas an increase in OEF would have been expected. If the OEF had remained constant across the different dose levels, we would nevertheless have anticipated an increase in OEF post-radiotherapy. However, the difference in OEF before and after radiotherapy in healthy tissue was not significant, while $CMRO_2$ did increase significantly. This would

mean that CBF had also been increased, which is contrary to what literature suggests. For better and more reliable results in future research, an improvement of the scanning pipeline would be of great interest to better investigate changes in metabolism and to create more reliable QSM maps and OEF and $CMRO_2$ maps accordingly.

Nevertheless, the data provides a clear implication of the use of OEF and $CMRO_2$ and their change after radiotherapy as well as their importance as biomarkers for general tissue healthy and indication of malignant areas.

REFERENCES

[1] S. Fantini, A. Sassaroli, K. T. Tgavalekos, and J. Kornbluth, "Cerebral blood flow and autoregulation: current measurement techniques and prospects for noninvasive optical methods," *Neurophotonics*, vol. 3, no. 3, p. 031411, 2016, doi: 10.1117/1.nph.3.3.031411.

[2] Z. B. Rodgers, J. A. Detre, and F. W. Wehrli, "MRI-based methods for quantification of the cerebral metabolic rate of oxygen," *J. Cereb. Blood Flow Metab.*, vol. 36, no. 7, pp. 1165–1185, 2016, doi: 10.1177/0271678X16643090.

[3] F. Xu, Y. Ge, and H. Lu, "Noninvasive quantification of whole-brain cerebral metabolic rate of oxygen (CMRO2) by MRI," *Magnetic Resonance in Medicine*, vol. 62, no. 1. pp. 141–148, 2009, doi: 10.1002/mrm.21994.

[4] J. H. Choi and M. S. Kim, "Homeostatic Regulation of Glucose Metabolism by the Central Nervous System," *Endocrinol. Metab.*, vol. 37, no. 1, pp. 9–25, 2022, doi: 10.3803/ENM.2021.1364.

[5] S. Agnihotri and G. Zadeh, "Metabolic reprogramming in glioblastoma: The influence of cancer metabolism on epigenetics and unanswered questions," *Neuro. Oncol.*, vol. 18, no. 2, pp. 160–172, 2016, doi: 10.1093/neuonc/nov125.

[6] J. P. Muizelaar and M. L. Schroder, "Overview of monitoring of cerebral blood flow and metabolism after severe head injury," *Can. J. Neurol. Sci.*, vol. 21, no. SUPPL. 1, pp. 6–11, 1994, doi: 10.1017/s0084255900003685.

[7] R. J. DeBerardinis and K. R. Keshari, "Metabolic analysis as a driver for discovery, diagnosis, and therapy," *Cell*, vol. 185, no. 15, pp. 2678–2689, 2022, doi: 10.1016/j.cell.2022.06.029.

[8] P. Ekkekakis, E. E. Hall, and S. J. Petruzzello, "Practical markers of the transition from aerobic to anaerobic metabolism during exercise: Rationale and a case for affect-based exercise prescription," *Prev. Med. (Baltim).*, vol. 38, no. 2, pp. 149–159, 2004, doi: 10.1016/j.ypmed.2003.09.038.

[9] Y. W. Junghun Cho, Youngwook Kee, Pasal Spincemaille, Thanh Nguyen, Jingwei Zhang, Ajay Gupta, Shun Zhang, "Cerebral Metabolic Rate of Oxygen (CMRO2) Mapping by Combining Quantitative Susceptibility Mapping (QSM) and Quantitative Blood Oxygenation Level Dependent Imaging (qBOLD)," *Magn. Reson. Med.*, vol. 80, no. 4, pp. 1595–1604, 2018.

[10] M. A. Feitelson *et al.*, "Sustained proliferation in cancer: therapeutic targets," *Semin. Cancer Biol.*, vol. 35, pp. 25–54, 2016, doi: 10.1016/j.semcancer.2015.02.006.Sustained.

[11] D. W. Siemann, "The unique characteristics of tumor vasculature and preclinical evidence for its selective disruption by Tumor-Vascular Disrupting Agents," *Cancer Treat. Rev.*, vol. 37, no. 1, pp. 63–74, 2011, doi: 10.1016/j.ctrv.2010.05.001.

[12] P. L. Y. Tang, A. Méndez Romero, J. P. M. Jaspers, and E. A. H. Warnert, "The potential of advanced MR techniques for precision radiotherapy of glioblastoma," *Magn. Reson. Mater. Physics, Biol. Med.*, vol. 35, no. 1, pp. 127–143, 2022, doi: 10.1007/s10334-021-00997-y.

[13] H. J. Park, R. J. Griffin, S. Hui, S. H. Levitt, and C. W. Song, "Radiation-induced vascular damage in tumors: Implications of vascular damage in ablative hypofractionated radiotherapy (SBRT and SRS)," *Radiat. Res.*, vol. 177, no. 3, pp. 311–327, 2012, doi: 10.1667/RR2773.1.

[14] C. Hou, G. Gong, L. Wang, Y. Su, J. Lu, and Y. Yin, "The Study of Cerebral Blood Flow Variations during Brain Metastases Radiotherapy," *Oncol. Res. Treat.*, vol. 45, no. 3, pp. 130–137, 2022, doi: 10.1159/000521291.

[15] S. J. Haikerwal, J. Hagekyriakou, M. MacManus, O. A. Martin, and N. M. Haynes, "Building immunity to cancer with radiation therapy," *Cancer Lett.*, vol. 368, no. 2, pp. 198–208, 2015, doi: 10.1016/j.canlet.2015.01.009.

[16] D. Jiang and H. Lu, "Cerebral oxygen extraction fraction MRI: Techniques and applications," *Magn. Reson. Med.*, vol. 88, no. 2, pp. 575–600, 2022, doi: 10.1002/mrm.29272.

[17] J. Aanerud *et al.*, "Brain energy metabolism and blood flow differences in healthy aging," *J. Cereb. Blood Flow Metab.*, vol. 32, no. 7, pp. 1177–1187, 2012, doi: 10.1038/jcbfm.2012.18.

[18] J. P. Bremmer *et al.*, "Day-to-day test-retest variability of CBF, CMRO2, and OEF measurements using dynamic 15O PET studies," *Mol. Imaging Biol.*, vol. 13, no. 4, pp. 759–768, 2011, doi: 10.1007/s11307-010-0382-1.

[19] J. M. Murkin, "Cerebral autoregulation: The role of CO2 in metabolic homeostasis," *Semin. Cardiothorac. Vasc. Anesth.*, vol. 11, no. 4, pp. 269–273, 2007, doi: 10.1177/1089253207311159.

[20] R. J. Deberardinis and D. Ph, "Tumor Microenvironment , Metabolism , and Immunotherapy," pp. 869–871, 2020.

[21] M. V. Liberti and J. W. Locasale, "The Warburg Effect: How Does it Benefit Cancer Cells?," *Trends Biochem. Sci.*, vol. 41, no. 3, pp. 211–218, 2016, doi: 10.1016/j.tibs.2015.12.001.

[22] J. Cho, J. Lee, H. An, M. S. Goyal, Y. Su, and Y. Wang, "Cerebral oxygen extraction fraction (OEF): Comparison of challenge-free gradient echo QSM+qBOLD (QQ) with 15O PET in healthy adults," *J. Cereb. Blood Flow Metab.*, vol. 41, no. 7, pp. 1658–1668, 2021, doi: 10.1177/0271678X20973951.

[23] J. Cho, P. Spincemaille, T. D. Nguyen, A. Gupta, and Y. Wang, "Temporal clustering, tissue composition, and total variation for mapping oxygen extraction fraction using QSM and quantitative BOLD," *Magn. Reson. Med.*, vol. 86, no. 5, pp. 2635–2646, 2021, doi: 10.1002/mrm.28875.

[24] J. Liu *et al.*, "Morphology enabled dipole inversion for quantitative susceptibility mapping using structural consistency between the magnitude image and the susceptibility map," *Neuroimage*, vol. 59, no. 3, pp. 2560–2568, 2012, doi: 10.1016/j.neuroimage.2011.08.082.

[25] T. Liu *et al.*, "A novel background field removal method for MRI using projection onto dipole fields (PDF)," *NMR Biomed.*, vol. 24, no. 9, pp. 1129–1136, Nov. 2011, doi: 10.1002/nbm.1670.

[26] K. S. Chan and J. P. Marques, "SEPIA—Susceptibility mapping pipeline tool for phase images," *Neuroimage*, vol. 227, no. November 2020, p. 117611, 2021, doi: 10.1016/j.neuroimage.2020.117611.

[27] S. Zhang *et al.*, "Initial Experience of Challenge-Free MRI-Based Oxygen Extraction Fraction Mapping of Ischemic Stroke at Various Stages: Comparison With Perfusion and Diffusion Mapping," *Front. Neurosci.*, vol. 14, no. September, pp. 1–11, 2020, doi: 10.3389/fnins.2020.535441.

[28] P. Schmidt, "Bayesian inference for structured additive regression models for large-scale problems with applications to medical imaging. Dissertation, LMU München: Faculty of Mathematics, Computer Science and

Statistics," *LudwigMaximilians-Universität München*, no. November, p. Chapter 6.1, 2016, [Online]. Available: https://edoc.ub.uni-muenchen.de/20373/.

[29] M. Jenkinson, M. Pechaud, and S. Smith, "BET2-MR-Based Estimation of Brain, Skull and Scalp Surfaces," *Hum. Brain Mapp.*, vol. 17, no. 2, pp. 143–155, 2002, [Online]. Available: www.fmrib.ox.ac.uk/analysis/research/bet.

[30] S. M. Smith, "Fast robust automated brain extraction," *Hum. Brain Mapp.*, vol. 17, no. 3, pp. 143–155, 2002, doi: 10.1002/hbm.10062.

[31] P. A. Yushkevich *et al.*, "User-guided 3D active contour segmentation of anatomical structures: Significantly improved efficiency and reliability," *Neuroimage*, vol. 31, no. 3, pp. 1116–1128, 2006, doi: 10.1016/j.neuroimage.2006.01.015.

[32] Y. Zhang, M. Brady, and S. Smith, "Segmentation of brain MR images through a hidden Markov random field model and the expectation-maximization algorithm," *IEEE Trans. Med. Imaging*, vol. 20, no. 1, pp. 45–57, 2001, doi: 10.1109/42.906424.

[33] M. Jenkinson and S. Smith, "A global optimisation method for robust affine registration of brain images," *Med. Image Anal.*, vol. 5, no. 2, pp. 143–156, 2001, doi: 10.1016/S1361-8415(01)00036-6.

[34] M. Jenkinson, P. Bannister, M. Brady, and S. Smith, "Improved Optimization for the Robust and Accurate Linear Registration and Motion Correction of Brain Images," *Neuroimage*, vol. 17, no. 2, pp. 825–841, 2002, doi: 10.1006/nimg.2002.1132.

[35] S. C. Formenti and S. Demaria, "Systemic effects of local radiotherapy," *Lancet Oncol.*, vol. 10, no. 7, pp. 718–726, 2009, doi: 10.1016/S1470-2045(09)70082-8.

[36] P. Mehnati, B. Baradaran, F. Vahidian, and S. Nadiriazam, "Functional response difference between diabetic/normal cancerous patients to inflammatory cytokines and oxidative stresses after radiotherapy," *Reports Pract. Oncol. Radiother.*, vol. 25, no. 5, pp. 730–737, 2020, doi: 10.1016/j.rpor.2020.06.008.

[37] S. Siva, M. P. MacManus, R. F. Martin, and O. A. Martin, "Abscopal effects of radiation therapy: A clinical review for the radiobiologist," *Cancer Lett.*, vol. 356, no. 1, pp. 82–90, 2015, doi: 10.1016/j.canlet.2013.09.018.

[38] A. R. Zazulia *et al.*, "Hypoperfusion without ischemia surrounding acute intracerebral hemorrhage," *J. Cereb. Blood Flow Metab.*, vol. 21, no. 7, pp. 804–810, 2001, doi: 10.1097/00004647-200107000-00005.

[39] G. Xi, R. F. Keep, and J. T. Hoff, "Pathophysiology of brain edema formation," *Neurosurg. Clin. N. Am.*, vol. 13, no. 3, pp. 371–383, 2002, doi: 10.1016/S1042-3680(02)00007-4.

[40] S. Taki *et al.*, "Changes in regional cerebral blood flow in irradiated regions and normal brain after stereotactic radiosurgery," *Ann. Nucl. Med.*, vol. 16, no. 4, pp. 273–277, 2002, doi: 10.1007/BF03000106.

[41] T. Hamada, T. Kaku, S. Mitsu, Y. Morita, N. Ohno, and H. Yamaguchi, "Lactic Acidosis and Hypoglycemia in a Patient with Gastric Diffuse Large B-Cell Lymphoma due to the Warburg Effect," *Case Rep. Oncol.*, vol. 13, no. 2, pp. 1047–1052, 2020, doi: 10.1159/000509510.

[42] V. Khlebnikov, J. C. W. Siero, A. A. Bhogal, P. R. Luijten, D. W. J. Klomp, and H. Hoogduin, "Establishing upper limits on neuronal activity–evoked pH changes with APT-CEST MRI at 7 T," *Magn. Reson. Med.*, vol. 80, no. 1, pp. 126–136, 2018, doi: 10.1002/mrm.27013.

[43] J. A. Kellum, M. Song, and J. Li, "Science review: Extracellular acidosis and the immune response: Clinical and physiologic implications," *Crit. Care*,

vol. 8, no. 5, pp. 331–336, 2004, doi: 10.1186/cc2900.

[44] L. Serrano Cardona and E. Muñoz Mata, “Imaging of Brain Tumors: MR Spectroscopy and Metabolic Imaging,” *Neuroimaging Clin. N. Am.*, vol. 83, no. 1, pp. 1–11, 2013, doi: 10.1016/j.nic.2010.04.003.Imaging.

[45] H. M. De Feyter *et al.*, “Deuterium metabolic imaging (DMI) for MRI-based 3D mapping of metabolism in vivo,” *Sci. Adv.*, vol. 4, no. 8, pp. 1–12, 2018, doi: 10.1126/sciadv.aat7314.

APPENDIX A

OVERVIEW OF INCLUDED PATIENT DATA

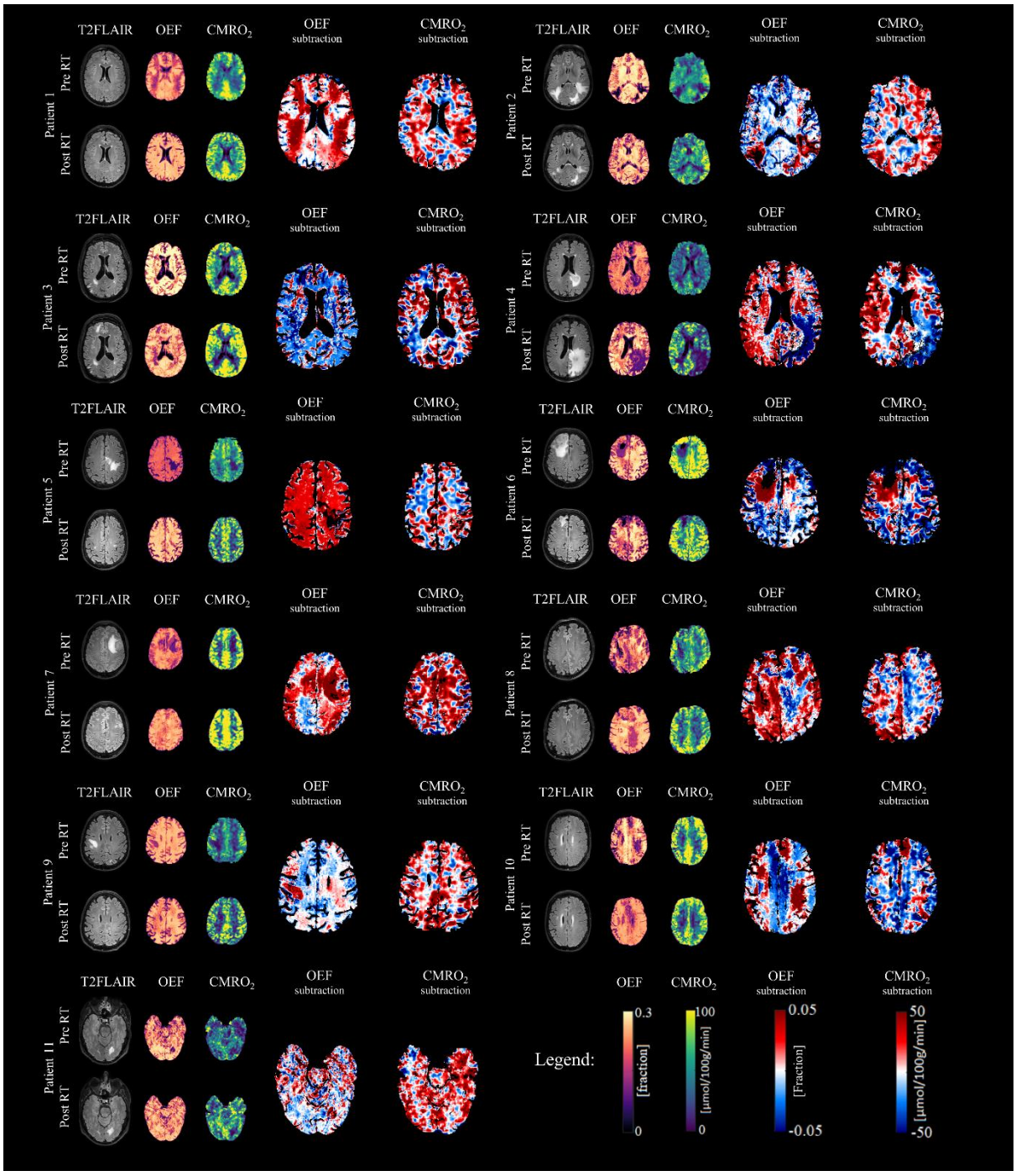

Figure 8: Overview of T2FLAIR, OEF, CMRO2 and subtraction maps for all eleven patients involved in the dataset

APPENDIX B

ADDITIONAL EVALUATION OF STATISTICAL ANALYSES

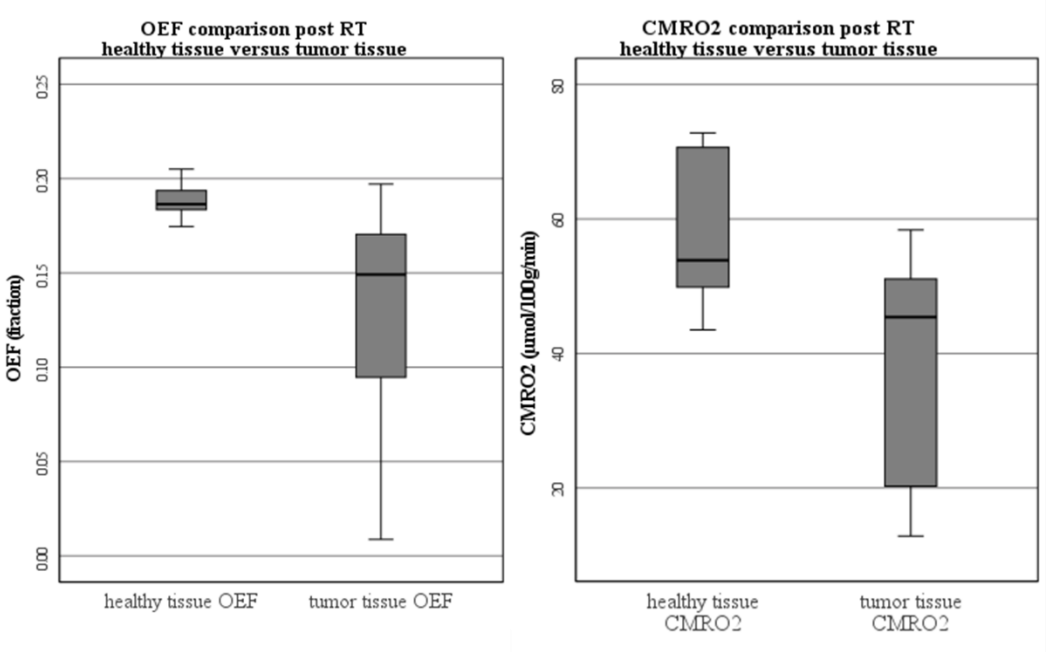

Figure 9: Boxplot of statistical analysis part A; Malignant tissue compared to healthy tissue after radiotherapy. Results indicate that OEF is significantly higher in healthy tissue compared to tumor tissue (Z = -2.028, p < 0.05). CMRO2 yielded a nonsignificant difference between healthy tissue and tumor tissue (Z = -1.782, p = 0.075). These results showed a similar tendency to the pre-radiotherapy results in healthy tissue versus tumor tissue OEF and CMRO2.

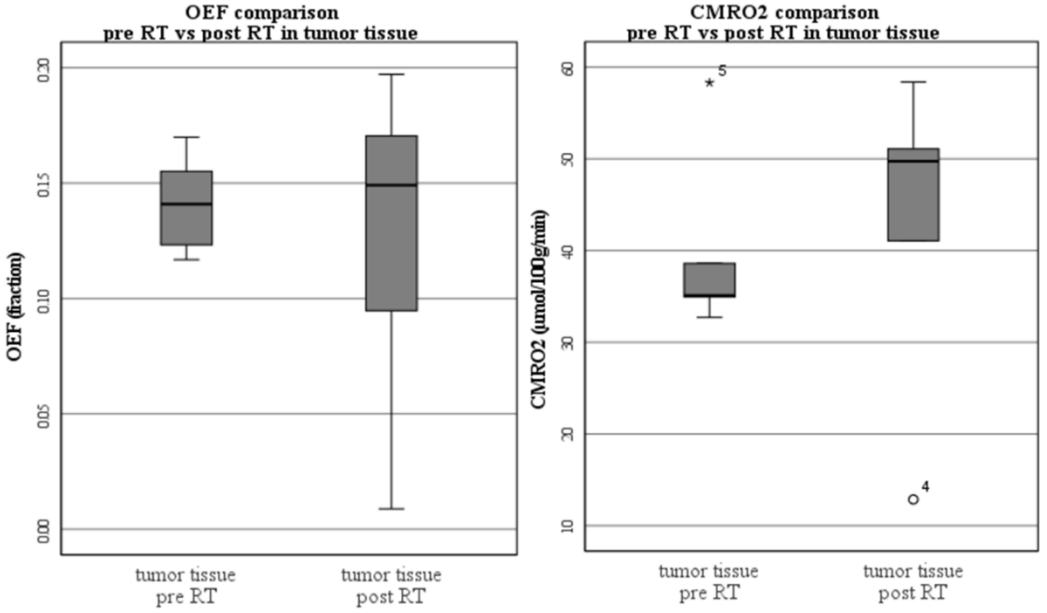

Figure 10: Boxplots of statistical analysis part B; The change in OEF and CMRO2 values in malignant tissue before and after radiotherapy. Results indicate that both OEF and CMRO2 do not significantly differ between pre- and post-radiotherapy (Z = -0.579, p = 0.562) and (Z = -0.405, p = 0.686), respectively.

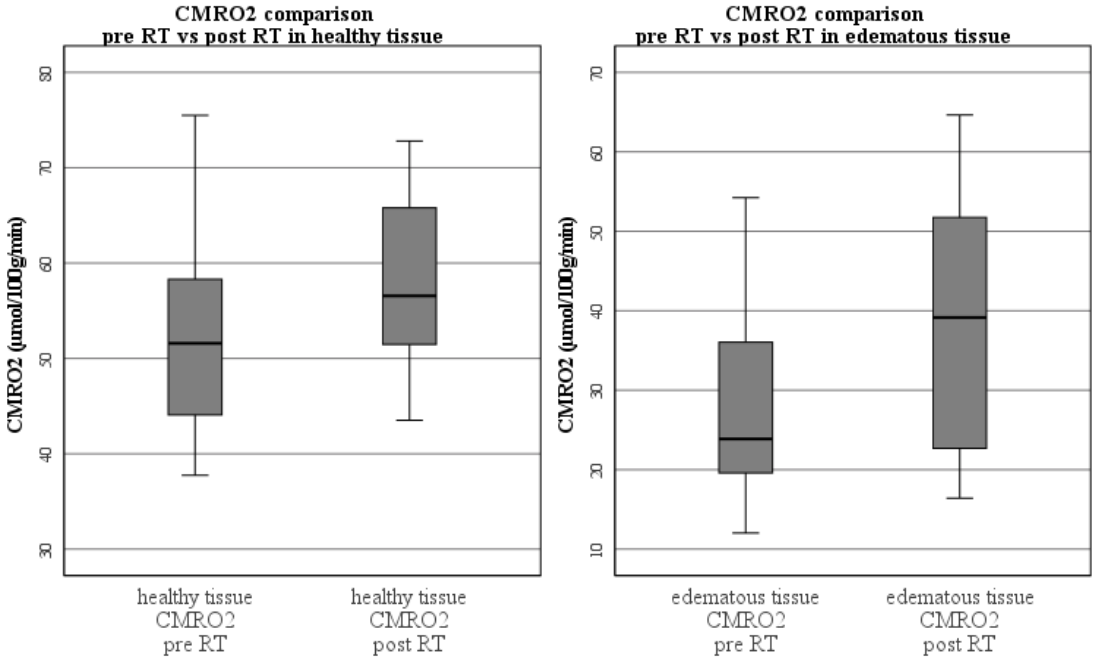

Figure 11: Boxplots of the additional statistical analysis part C; Further evaluation of the comparison of CMRO2 in healthy- and edematous tissue prior to radiotherapy compared to after radiotherapy. With the applied Bonferroni correction of alpha = 0.025, the Wilcoxon signed-rank tests showed no significant results for either healthy tissue or edematous tissue, (Z = -2.045, p = 0.026) and (Z = -1.274, p = 0.203), respectively.